

A. Colliander, S. Tauriainen, T. Auer, J. Kainulainen, J. Uusitalo, M. Toikka, M. T. Hallikainen, MIRAS Reference Radiometer: A Fully Polarimetric Noise Injection Radiometer, IEEE Transactions on Geoscience and Remote Sensing, vol. 43, no. 5, pp. 1135-1143, May 2005.

© 2005 IEEE

Reprinted with permission.

This material is posted here with permission of the IEEE. Such permission of the IEEE does not in any way imply IEEE endorsement of any of Helsinki University of Technology's products or services. Internal or personal use of this material is permitted. However, permission to reprint/republish this material for advertising or promotional purposes or for creating new collective works for resale or redistribution must be obtained from the IEEE by writing to [pubs-permissions@ieee.org](mailto:pubs-permissions@ieee.org).

By choosing to view this document, you agree to all provisions of the copyright laws protecting it.

# MIRAS Reference Radiometer: A Fully Polarimetric Noise Injection Radiometer

Andreas Colliander, *Student Member, IEEE*, Simo Tauriainen, Tuomo I. Auer, Juha Kainulainen, Josu Uusitalo, Martti Toikka, and Martti T. Hallikainen, *Fellow, IEEE*

**Abstract**—A prototype reference radiometer for the Microwave Imaging Radiometer Using Aperture Synthesis (MIRAS) instrument of the Soil Moisture and Ocean Salinity satellite has been developed. The reference radiometer is an L-band fully polarimetric noise injection radiometer (NIR). The main purposes of the NIR are: 1) to provide precise measurement of the average fully polarimetric brightness temperature scene for absolute calibration of the MIRAS image map and 2) to measure the noise temperature level of the noise distribution network of the MIRAS for individual receiver calibration. The performance of the NIR is a decisive factor of the MIRAS performance. In this paper we present the operation principles and calibration procedures of the NIR, a measurement technique called blind correlation making measurements of full Stokes vector possible with the noise injection method, and finally experimental results verifying certain aspects of the design.

**Index Terms**—Digital correlation, noise injection radiometer (NIR), polarimetric radiometer, Stokes parameters.

## I. INTRODUCTION

THE Microwave Imaging Radiometer Using Aperture Synthesis (MIRAS) instrument is the single payload of the Soil Moisture and Ocean Salinity (SMOS) mission of European Space Agency (ESA) [1], [2]. MIRAS is an interferometric radiometer providing brightness temperature images of earth's surface at L-band. The calibration procedure of the MIRAS involves three reference radiometers, which are to provide a fully polarimetric reference for the absolute calibration of the MIRAS image map. Additionally, it is to measure the noise temperature level of the noise distribution network (NDN), which is used for individual receiver calibration.

The reference radiometer is a fully polarimetric noise injection radiometer (NIR) with the capability to measure the noise temperature level of the NDN. The NIR can also be used in the MIRAS array as a regular receiver unit for the formation of the interferometric image.

Manuscript received May 16, 2004; revised October 9, 2004. This work was supported in part by the European Aeronautic Defence and Space Company (EADS-CASA) and in part by the European Space Agency as part of MDPP-2 Contract DE01/B-350/P.

A. Colliander, S. Tauriainen, T. I. Auer, J. Kainulainen, and M. T. Hallikainen are with the Laboratory of Space Technology, Helsinki University of Technology, FIN-02015 HUT, Finland (e-mail: andreas.colliander@hut.fi; simo.tauriainen@hut.fi; tuomo.auer@hut.fi; juha.kainulainen@avasun.hut.fi; martti.hallikainen@hut.fi).

J. Uusitalo is with the Ylinen Electronics Ltd, FIN-02700 Kauniainen, Finland (e-mail: josuuusitalo@ylinen.fi).

M. Toikka is with the Toikka Engineering Ltd, FIN-02360 Espoo, Finland (e-mail: toikka@co.inet.fi).

Digital Object Identifier 10.1109/TGRS.2004.840667

Fully polarimetric radiometers measure the so-called modified Stokes parameters, which are defined under the Rayleigh-Jeans approximation as [4]

$$\mathbf{T} = \begin{bmatrix} T_v \\ T_h \\ T_3 \\ T_4 \end{bmatrix} = \frac{\lambda^2}{k_B \eta B} \begin{bmatrix} \langle |E_v|^2 \rangle \\ \langle |E_h|^2 \rangle \\ 2\Re \langle E_v E_h^* \rangle \\ 2\Im \langle E_v E_h^* \rangle \end{bmatrix} \quad (1)$$

where  $T_v$ ,  $T_h$ ,  $T_3$ , and  $T_4$  are the brightness temperatures of the vertically and horizontally polarized radiation and third and fourth Stokes parameter, respectively;  $\lambda$  is the wavelength;  $k_B$  is the Boltzmann's constant;  $\eta$  is the impedance of the medium;  $B$  is the bandwidth; and  $E_v$  and  $E_h$  are the vertically and horizontally polarized electric fields. The brackets stand for infinite time average.

There are many techniques to measure all four Stokes parameters. This NIR design uses a one-bit/two-level digital correlator, the same one that is used for MIRAS imaging. Digital correlators has been previously used in polarimetric radiometers, but the challenge in the implemented method is the fact that there is additional noise in the correlated signal due to the noise injection method. However, the noise injection method was selected to meet the high requirements set for the reference radiometer arising especially from the goal of ocean surface salinity measurement.

The precision of a noise injection radiometer is based on comparing the measured signal to two reference sources, the noise temperatures of which are known. This will remove the effect of the receiver gain and offset variations. The antenna temperature can be solved from the length of the noise pulse, since the level of the noise is determined in calibration [3].

## II. OPERATION OF NIR

NIR has several operational modes, but the most important for the object of this paper are the following: total power mode for antenna measurement (NIR-TP), noise injection mode for antenna measurement (NIR-A), noise injection mode for the NDN measurement (NIR-R), and the mode for calibration of NIR-R mode (REF-CAL). Fig. 1 presents a schematic diagram of the power detector output of one receiver in NIR-A, NIR-R, and REF-CAL modes.

The NIR-A mode operation is based on the following equation:

$$T_U = \tau(T_A + T_{NA}) + (1 - \tau)T_A \quad (2)$$

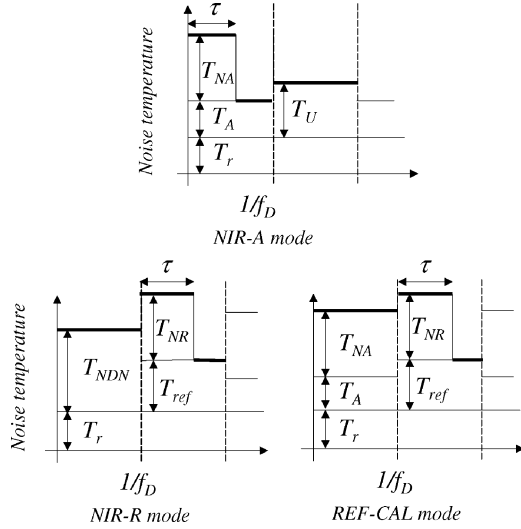


Fig. 1. Operational modes of the NIR for one receiver. NIR-A mode is for measuring the antenna temperature, NIR-R mode for measuring the noise temperature of the NDN, and REF-CAL mode is for calibration of the NIR-R mode. One Dicke cycle is the period  $1/f_D$ , and  $\tau$  is the length of the noise injection. See text for explanation of other symbols.

where  $T_U$  is the Dicke reference load (or U-load) noise temperature,  $T_A$  is the antenna temperature of the receiver,  $T_{NA}$  is the noise temperature of the noise injection of the receiver, and  $\tau$  is the length of the noise injection as a fraction of half of the Dicke cycle.

The NIR-R mode works under the subsequent equation

$$T_{NDN} = \tau(T_{ref} + T_{NR}) + (1 - \tau)T_{ref} \quad (3)$$

where  $T_{NDN}$  is the noise temperature of the MIRAS noise distribution network,  $T_{ref}$  is the noise temperature of the reference branch without the noise injection, and  $T_{NR}$  is the noise temperature of the reference noise injection.

The REF-CAL mode follows the next rule

$$T_A + T_{NA} = \tau(T_{ref} + T_{NR}) + (1 - \tau)T_{ref} \quad (4)$$

from which the reference noise injection  $T_{NR}$  can be solved when the antenna temperature  $T_A$  and antenna noise injection  $T_{NA}$  are known. Note that in the REF-CAL mode noise is injected during the entire antenna measurement time.

### III. MEASURING FULLY POLARIMETRIC BRIGHTNESS TEMPERATURE

#### A. Horizontal and Vertical Polarization

The antenna brightness temperature is basically retrieved from the knowledge of the noise injection temperature and physical temperature of the U-load.

Starting from (2) an equation for antenna temperature  $T_A$  taking the losses of the antenna and the network connecting it to the receivers into account can be written as (see Appendix for details)

$$T_A = a\tau + b \quad (5)$$

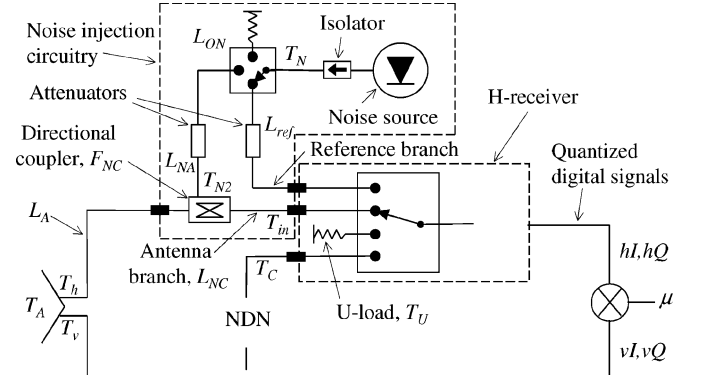


Fig. 2. Schematic diagram of NIR  $h$ -channel. The  $v$ -channel is omitted due to the fact that it is identical to the  $h$ -channel.

where

$$a = \frac{L_A}{1 - F_{NC}} \left( \frac{T_N + T_{p3}}{L_{NA}L_{ON}} \right) \quad (6)$$

and

$$b = \frac{F_{NC}L_A}{F_{NC} - 1} \left\{ L_{NC}T_U - \frac{T_{p3}}{F_{NC}} - \left[ \left( 1 + \frac{1}{F_{NC}} \right) \left( 1 - \frac{1}{L_{NC}} \right) + L_{NC} - 1 \right] T_{p5} \right\}. \quad (7)$$

In the above equations  $F_{NC}$  is the coupling factor of the directional coupler,  $T_{p5}$  is its physical temperature, and  $L_{NC}$  is the insertion loss of the coupler and loss of the cable connecting it to the receiver;  $L_A$  is the loss of the antenna and its connection network;  $T_N$  is the noise temperature of the noise source;  $L_{NA}$  is the attenuation of the attenuator in the injection channel, and  $T_{p3}$  is its physical temperature; and  $L_{ON}$  is the insertion loss of the switch when the switch is connected to the injection channel. See also Fig. 2.

#### B. Third and Fourth Stokes Parameter

Consider an ideal completely noise free total power radiometer with receivers for  $h$ - and  $v$ -polarization and correlator for retrieving the complex correlation between the two. Then the third and fourth Stokes parameter can be solved using this ideal complex correlation  $\mu_0$  as follows:

$$T_3 = 2\sqrt{T_v T_h} \Re\{\mu_0\} \quad (8)$$

$$T_4 = 2\sqrt{T_v T_h} \Im\{\mu_0\}. \quad (9)$$

When the Stokes parameters are measured with noisy receivers, the receiver noise temperature is taken into account using the so-called modulus term  $\tilde{g}$  so that (e.g., [8])

$$\mu = \mu_{ThIv} + j\mu_{QhIv} = \tilde{g}\mu_0 \quad (10)$$

where the real part of the nominal correlation coefficient  $\mu_{ThIv}$  is the correlation between the in-phase outputs of the receivers, and the imaginary part  $\mu_{QhIv}$  is the correlation between the quadrature output of the  $h$ -receiver and the in-phase output of the  $v$ -receiver.

Additionally, when the Stokes parameters are measured during a noise injection measurement the modulus term is written so that

the injected noise is taken into account as increased receiver noise temperature. These two cases are discussed below.

1) *Stokes Parameters in Total Power Measurement*: MIRAS measures the normalized complex correlation of two receivers using 1-bit/2-level digital correlators. This gives correlation value according to the following equation [5]:

$$Z = \frac{1}{N} \sum_{i=1}^N \text{sign}(x(t_i))\text{sign}(y(t_i)) \quad (11)$$

in which  $x(t_i)$  and  $y(t_i)$  are the input signal samples of the two receivers and  $N$  is the number of the samples being correlated. This digital correlation value is related to the analogue correlation value, when it is applied to the signal which has limited spectrum, as [6]

$$\mu = \sin\left(\frac{\pi}{2}Z\right) \quad (12)$$

where  $\mu$  is called here as the measured correlation coefficient.

The ideal correlation coefficient (measured with a noise free receiver) is retrieved from the measured one using the relation

$$\mu = \tilde{g}\mu_0 \quad (13)$$

where  $\mu_0$  is the ideal correlation coefficient and  $\tilde{g}$  is the modulus term defined as

$$\tilde{g} = g_{FW} \sqrt{\frac{T_v}{T_v + T_{rv}}} \sqrt{\frac{T_h}{T_h + T_{rh}}} \quad (14)$$

where  $T_{rv}$  and  $T_{rh}$  are the receiver noise temperatures of the  $v$ - and  $h$ -receiver, respectively, and  $g_{FW}$  is the fringe-washing factor, which describes the frequency response relations of the receivers.

Redundant correlation coefficient, the complex conjugate of the nominal, is the one in which the real part  $\mu_{QhQv}$  is the correlation between the quadrature outputs, and the imaginary part  $\mu_{IhQv}$  is the correlation between the in-phase output of the  $h$ -receiver and the quadrature output of the  $v$ -receiver.

2) *Solving Stokes Parameters With Noise Injection*: In noise injection measurement the Dicke cycle is divided into four steps in order to take into account the different amount of noise present during the measurement of correlation. The time steps are defined here as follows:

- 1) measurement with noise injection to both channels;
- 2) measurement with noise injection to one channel;
- 3) measurement without noise injection;
- 4) measurement of the Dicke load (zero correlation).

The measured correlation coefficient is now written for every time step  $p = 1, 2, 3, 4$  yielding

$$\mu_p = \sin\left(\frac{\pi}{2}Z_p\right) \quad (15)$$

where  $\mu_p$  is the measured correlation coefficient and

$$Z_p = \frac{1}{N_p} \sum_{i=1}^{N_p} \text{sign}(x(t_i))\text{sign}(y(t_i)) \quad (16)$$

in which  $x(t_i)$  and  $y(t_i)$  are the input signal samples of the two receivers and  $N_p$  is the number of the samples being correlated during the time step.

The ideal correlation coefficient of a time step is retrieved from the measured one using the subsequent relation

$$\mu_p = \tilde{g}_p\mu_0. \quad (17)$$

Since  $\mu_p$  is written for every time step, it yields for the total correlation coefficient

$$\mu = \sin\left(\frac{\pi}{2} \sum_{p=1}^4 \frac{N_p}{N} Z_p\right) \quad (18)$$

which, using (15), can be written as

$$\mu = \sin\left(\sum_{p=1}^4 \frac{N_p}{N} \sin^{-1}(\tilde{g}_p\mu_0)\right) \quad (19)$$

from which  $\mu_0$  can be solved numerically.

Finally, the modulus terms are written for each time steps as follows:

$$\tilde{g}_1 = g_{FW} \sqrt{\frac{T_v}{T_v + T_{rv} + T_{Nv}}} \sqrt{\frac{T_h}{T_h + T_{rh} + T_{Nh}}} \quad (20)$$

$$\tilde{g}_2 = g_{FW} \sqrt{\frac{T_v}{T_v + T_{rv} + T_{Nv}}} \sqrt{\frac{T_h}{T_h + T_{rh}}} \quad (21)$$

$$\tilde{g}_3 = g_{FW} \sqrt{\frac{T_v}{T_v + T_{rv}}} \sqrt{\frac{T_h}{T_h + T_{rh}}} \quad (22)$$

where  $T_{Nv}$  and  $T_{Nh}$  are the noise temperatures of the noise injections of the  $v$ - and  $h$ -receiver, respectively. The equations hold when the noise injection is longer in the  $v$ -receiver. If the noise injection is longer in the horizontal receiver, the subscript  $v$  is interchanged with the subscript  $h$  in (21).

#### IV. MEASURING MIRAS BASELINE WITH NIR

Each channel of the NIR can form an interferometer baseline with each of the receivers of the MIRAS. These baselines need also application of blind correlation concept so that the noise injection in the NIR channel is taken into account in the modulus term.

For the formulation, the Dicke cycle of the NIR is divided into three steps in the following manner (the normal receiver measures the antenna during the whole Dicke cycle of the NIR):

- 1) measurement with noise injection;
- 2) measurement without noise injection;
- 3) measurement of the Dicke load (zero correlation).

The correlation coefficient is now written taking the time steps into account

$$\mu = \sin\left(\sum_{p=1}^3 \frac{N_p}{N} \sin^{-1}(\tilde{g}_p\mu_0)\right). \quad (23)$$

Now the modulus terms are written as

$$\tilde{g}_1 = g_{FW} \sqrt{\frac{T_k}{T_k + T_{rk} + T_{Nk}}} \sqrt{\frac{T_j}{T_j + T_{rj}}} \quad (24)$$

$$\tilde{g}_2 = g_{FW} \sqrt{\frac{T_k}{T_k + T_{rk}}} \sqrt{\frac{T_j}{T_j + T_{rj}}} \quad (25)$$

where subscript  $k$  stands for a NIR channel and subscript  $j$  stands for a normal receiver.

## V. MEASURING NDN

The noise temperature of the NDN is measured in the NIR-R mode. Starting from (3) the nonidealities of the reference branch noise injection can be taken into account as follows (see the Appendix for details):

$$T_{NDN} = \tau \left( \frac{T_N - T_{p3}}{L_{ON} L_{ref}} + T_{p3} \right) + (1 - \tau) \left( T_{p3} + \frac{T_N - T_{p3}}{L_{OFF} L_{ref}} \right) \quad (26)$$

where  $L_{ref}$  is the attenuation of the attenuator in the reference channel,  $T_{p3}$  is its physical temperature, and  $L_{OFF}$  is the isolation of the noise injection switch. See also Fig. 2.

## VI. CALIBRATION OF NIR

### A. Precalibration of Correlation Coefficient

The calibration of correlation coefficient is done both by measuring NDN and external target. The calibration procedure is given below step by step.

1) *Normalized Quantizer Offset Voltages*: The normalized quantizer offset voltages are determined as [7]

$$\frac{a_i}{\sigma_i} = \sqrt{\frac{2}{\pi}} \mu_{i,0} \quad (27)$$

where  $a_i$  is the offset voltage of quantizer  $i$ ,  $\sigma_i$  is the standard deviation of the signal at the quantizer, and  $\mu_{i,0}$  is the measured correlation coefficient against all zeros signal. The offset can be determined at any time of NIR measurements, also during the measurement of NDN.

2) *Quadrature Error*: The quadrature error is the deviation of the phase difference of the in-phase (I) and quadrature (Q) outputs of a channel from  $90^\circ$ . First the quantizer offsets are accounted for by solving the following equation: [7]

$$\arcsin(\mu_{i,j}^{raw}) = \arcsin(\mu_{i,j}) - \frac{1}{2\sqrt{1 - \mu_{i,j}^2}} \left( \frac{\mu_{i,j} a_i^2}{\sigma_i^2} + \frac{\mu_{i,j} a_j^2}{\sigma_j^2} - \frac{2a_i a_j}{\sigma_j \sigma_i} \right) \quad (28)$$

where  $\mu_{i,j}^{raw}$  is the measured correlation and  $\mu_{i,j}$  is the true correlation of quantizer outputs  $i$  and  $j$ .

The quadrature errors are now solved for the  $v$ - and  $h$ -channels using the offset corrected correlation coefficients as follows:

$$\Theta_{vq} = -\arcsin(\mu_{IvQv}) \quad (29)$$

$$\Theta_{hq} = -\arcsin(\mu_{IhQh}) \quad (30)$$

where  $\mu_{IvQv}$  and  $\mu_{IhQh}$  are the correlation coefficients between  $I$ - and  $Q$ -outputs of the  $v$ - and  $h$ -channel, respectively, obtained during measurement of NDN.

3) *In-Phase Error*: The in-phase error between  $v$ - and  $h$ -channels is obtained from the phase of the complex correlation, after removing the quadrature errors as follows [8]:

$$\begin{bmatrix} \mu_{IhIv} \\ \mu_{QhIv} \end{bmatrix}_{new} = \mathbf{Q}^{-1} \begin{bmatrix} \mu_{IhIv} \\ \mu_{QhIv} \end{bmatrix}_{old} \quad (31)$$

where  $\mu_{IhIv}$  is the correlation coefficient between  $I$ -outputs of the  $v$ - and  $h$ -channel, and  $\mu_{QhIv}$  is the correlation coefficient

between  $Q$ -output of the  $h$ -channel and  $I$ -output of the  $v$ -channel obtained during the measurement of NDN; subscript *new* means quadrature error corrected correlation coefficients; subscript *old* means the quantizer offset corrected correlation coefficient and

$$\mathbf{Q}^{-1} = \frac{1}{\cos(\Theta_{qv})} \times \begin{bmatrix} \cos\left(\frac{1}{2}(\Theta_{qh} + \Theta_{qv})\right) & -\sin\left(\frac{1}{2}(\Theta_{qh} - \Theta_{qv})\right) \\ \sin\left(\frac{1}{2}(\Theta_{qh} + \Theta_{qv})\right) & \cos\left(\frac{1}{2}(\Theta_{qh} - \Theta_{qv})\right) \end{bmatrix}. \quad (32)$$

Note that the in-phase error solved this way, i.e., using the correlated noise from the NDN input port, does not take the imbalance of the NIR front-end cables into account. However, the front-end cables of NIR can be characterized with a known target, and since it is a passive network, it does not require as frequent calibration as the receiver part.

4) *Residual Offset*: There is a small offset, so-called residual offset, in the receivers due to thermal gradients, synchronous local oscillator leakage, and so on. This offset can be measured and compensated for by measuring the correlation coefficient from the internal matched loads (also called as uncorrelated loads or U-loads) of the receivers.

5) *Fringe-Washing Factor*: The fringe-washing function, which describes the difference between the frequency response of the receivers, can be measured with the correlator of the NIR since it has the property of correlating the signal with three different delays and thus the so-called 3-delay method [9] can be applied. The fringe-washing factor at certain delay  $t$  can be written as

$$g_{FW}(t) = \sqrt{\frac{T_{NDN} + T_{rh}}{T_{NDN}}} \sqrt{\frac{T_{NDN} + T_{rv}}{T_{NDN}}} \mu_{IhIv}(t) \quad (33)$$

in which  $t$  is  $+T$ ,  $0$  or  $-T$ ,  $T$  being 17.9 ns in the case of the correlator of the NIR. The three values of the fringe-washing function can be used to retrieve the whole function by fitting the values to a sinc-function as introduced in [9].

6) *Internal Self-Interference*: There is also self-interference in the noise injection circuitry due to cross-coupling from one channel to the other which is observed as an additional offset. This can also be measured by connecting uncorrelated loads to the antenna inputs of the receivers. However, since this effect is taken into account also in the measurement of overall self-interference it is not necessary to perform this measurement.

7) *Overall Self-Interference*: The overall self-interference is the internal self-interference combined to the external interference. The external self-interference consists of the correlation resulting from the cross-coupling of the noise injection from one channel to the other through the antenna. When measuring an uncorrelated target this effect can be measured. It should be noted that in the measurement also the internal self-interference adds to the measured correlation and thus the effect of overall self-interference is determined with one measurement. As internal self-interference, also the external self-interference is dependent on the level of the measured noise, and thus several levels of brightness temperature would be preferred for the measurement.

The following equation presents the principle of the self-interference. It is hard to define an equation for the internal self-in-

interference since the medium of coupling is not well-defined. The maximum overall self-interference can be written as

$$\mu_{\max} = \mu_{\text{int}}(\tau) + \mu_{\text{ext}}(\tau) \quad (34)$$

in which

$$\mu_{\text{ext}}(\tau) = \tau \frac{T_{NA}}{T_{NA} + T_A + T_r} \sqrt{\frac{|S_{hv}|^2}{I_{NC}}} \quad (35)$$

where  $S_{hv}$  is the isolation of the antenna channels and  $I_{NC}$  is the isolation of the directional coupler (with respect to coupling  $F_{NC}$ ).

### B. Calibration of Horizontal and Vertical Brightness Temperature

The NIR is calibrated using the so-called one-point calibration, meaning that only one target with known brightness temperature is used to determine the noise level of the noise injection, and thus the length of the noise injection pulse can be related to the antenna temperature.

When the NIR is measuring a known target  $T_{A0}$ , the noise temperature of the noise source can be solved from the following (see the Appendix for details):

$$T_N = L_{NA} L_{ON} \left[ \frac{F_{NC} - 1}{L_A} (b - T_A) \right] \frac{1}{\tau} - T_{p3}. \quad (36)$$

In order to solve  $T_N$  all the parameters in (36) need to be known. The coupling factor of the coupler  $F_{NC}$ , the attenuation of the attenuator in the antenna injection channel  $L_{NA}$ , and the insertion loss of the noise injection switch  $L_{ON}$  are required to be known only at moderate accuracy (in order of 1 dB) and are determined during the manufacturing of the radiometer with a vector network analyzer. Attenuations  $L_A$  and  $L_{NC}$  (included in parameter  $b$ ), on the other hand, need to be known with a good accuracy (in order of 0.01 dB). These are measured by radiometric measurements. The physical temperatures of the directional coupler  $T_{p5}$ , the attenuator in the noise injection channel  $T_{p3}$ , and the U-load  $T_U$  are measured using PT100 thermal sensors, which had accuracy of 0.1 K in the measurement range.

### C. Calibration of NDN Measurement

In order to calibrate the NIR-R mode the noise temperature of the reference branch noise injection is to be determined. This is done in the following manner: 1) a known target is measured in NIR-A mode so that the noise temperature of the antenna branch during the injection can be determined; and 2) the same target is measured in REF-CAL mode so that the noise temperature of the reference branch noise injection can be determined by relating it to the noise temperature of the antenna branch with full noise injection. See also Fig. 1.

The antenna branch noise level during the noise injection in the NIR-A mode can be solved from the following (see the Appendix for details):

$$T_{Aref} = \frac{T_U}{\tau} + \left(1 - \frac{1}{\tau}\right) \left\{ \frac{F_{NC} - 1}{F_{NC} L_{NC}} \left[ \frac{T_A}{L_A} + \left(1 - \frac{1}{L_A}\right) T_{p5} \right] + \frac{T_{p3}}{F_{NC} L_{NC}} + \left(1 - \frac{1}{L_{NC}}\right) T_{p5} \right\} \quad (37)$$

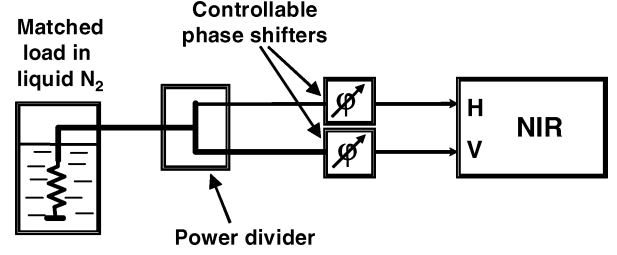


Fig. 3. Schematic diagram of the measurement setup for the correlation measurements.

for which the parameters are to be solved as in the case of NIR-A mode calibration presented in Section VI-B.

During the REF-CAL mode measurement the noise temperature of the noise source can be determined as follows (see the Appendix for details):

$$T_N = \frac{L_{ref}}{\frac{1}{L_{ON}} + \left(\frac{1}{\tau} - 1\right) \frac{1}{L_{OFF}}} \left\{ \frac{T_{Aref} - T_{p3}}{\tau} + \frac{T_{p3}}{L_{ref}} \left( \frac{1}{L_{ON}} + \frac{1 - \tau}{\tau L_{OFF}} \right) \right\} \quad (38)$$

for which the parameters are solved the same way as in the case of NIR-A mode calibration (Section VI-B).

This way the  $T_N$  can be determined for (26) for NDN measurement.

## VII. EXPERIMENTAL RESULTS

### A. Blind Correlation

1) *Measurement Setup*: Correlation measurements were carried out using the measurement setup presented in Fig. 3. In this measurement the idea is to be able to create a situation where NIR can see different Stokes parameters in any of its operational modes.

The noise temperature emitted by the cold load was determined by measuring the cable temperature distribution with five temperature sensors. Also the physical temperatures of the power divider and phase shifters were measured. In this way the inout noise temperature could be determined at all times during the measurements.

2) *Simulating Correlation Coefficient*: The results were also compared to the simulated correlation coefficient values calculated using the theory presented in [10]. In order to do the simulation the scattering parameters of the connecting network were measured with a vector network analyzer and the phase shifts of the phase shifters were determined using the correlator in-phase calibration.

3) *Measured Stokes Parameters*: Correlation coefficient was measured in different measurement modes as presented in Figs. 4 and 5. The magnitudes (i.e., the different radii in the figure) of the correlation coefficients depend on the ratio of the correlated noise and the total noise. The effect of the so-called blind correlation can be clearly seen. Furthermore, the Stokes parameters were solved using the previously presented equations yielding the results presented in Figs. 6 and 7. The simulations and the results obtained both in NIR-TP mode and in NIR-A mode are in good agreement.

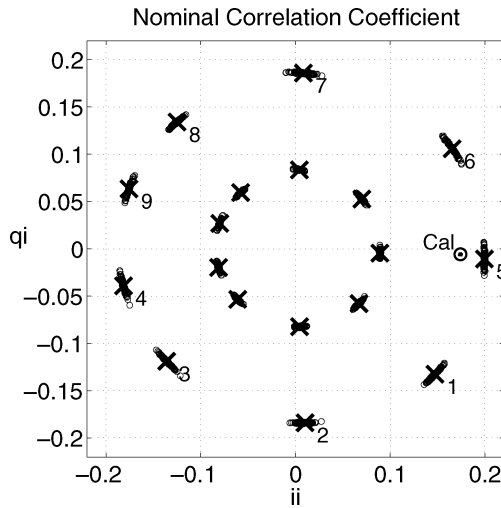


Fig. 4. Nominal correlation coefficient measured at different phase shifts between horizontal and vertical channels. The measurement used for offset and phase calibration is marked with text Cal. The coefficients on the outmost circle are measured in the NIR-TP mode and those on the innermost in the NIR-A mode.

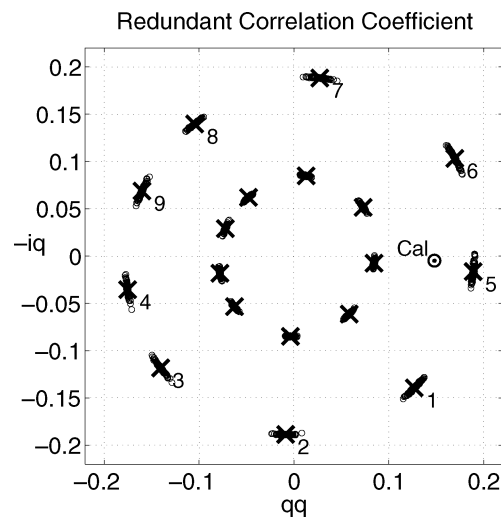


Fig. 5. Redundant correlation coefficient presented as in Fig. 4.

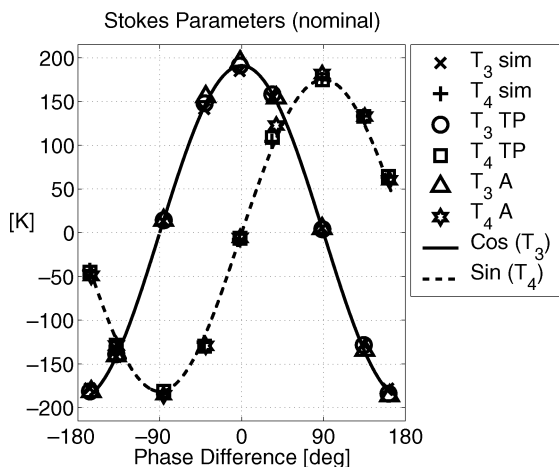


Fig. 6. Measured third and fourth Stokes parameters in NIR-TP (TP), NIR-A (A) operational modes, and the simulated Stokes parameters (sim) with Sin and Cos functions for illustration.

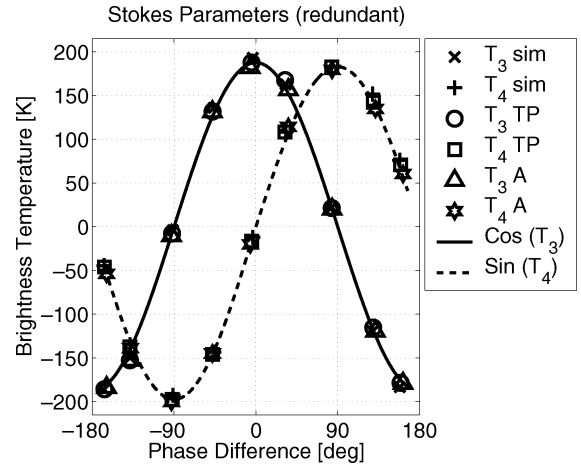


Fig. 7. Measured Stokes parameters using the redundant correlation coefficient. The results are presented as in Fig. 6.

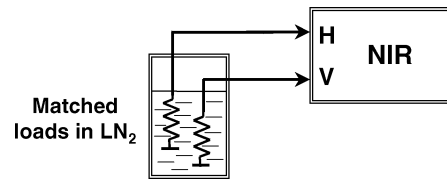


Fig. 8. Schematic diagram of the measurement setup for the measurements of an uncorrelated cold load.

B. Internal Self-Interference

1) *Measurement Setup:* For determining the internal self-interference, a cold uncorrelated target was connected to the antenna inputs of both channels of the NIR as depicted in Fig. 8. The physical temperature of the connecting cable of one of the loads was measured at five locations. The same temperature distribution was then considered to apply also for the other load, and thus the noise temperature emitted by the loads to the NIR could be determined.

2) *Results for Internal Self-Interference:* Although the internal self-interference is not strictly necessary to be determined it is interesting to compare it to the overall self-interference. Table I and Fig. 9 show NIR-A and NIR-TP mode measurement results of a cold uncorrelated target connected to the antenna inputs of both channels. Even after the removal of the residual offset there is offset in NIR-TP measurement. This is probably due to finite matching of the measured matched loads. The internal self-interference is solved by subtracting the offset measured in NIR-TP mode from the offset measured in NIR-A mode yielding  $-10.266$  c.u. ( $1 \text{ c.u.} = 10^{-4}$ ) and  $-4.164$  c.u. for  $\mu_{IhIv}$  and  $\mu_{QhIv}$ , respectively, being equal to the magnitude of  $11.01$  c.u. and phase of  $-157.9^\circ$  of complex correlation coefficient. This offset is applicable for input noise temperature of about  $90$  K, which was determined using the physical temperature measurements of the load.

Results presented in Table I also show that the standard deviation of the correlation coefficient measured in NIR-A mode is not degraded significantly when compared to that measured in the NIR-TP mode or from the U-load.

TABLE I  
CORRELATION COEFFICIENTS IN CORRELATION UNITS WHEN COLD UNCORRELATED TARGET OF MATCHED LOADS WERE MEASURED IN NIR-A AND NIR-TP MODES. MEASUREMENT FROM U-LOAD IS USED FOR THE RESIDUAL OFFSET CORRECTION

| Mode    | $\mu_{IhIv}$ | $\mu_{IhIv}$ | $\mu_{QhIv}$ | $\mu_{QhIv}$ |
|---------|--------------|--------------|--------------|--------------|
|         | mean         | std          | mean         | std          |
| NIR- A  | -12.655      | 4.237        | -1.329       | 4.271        |
| NIR- TP | -2.389       | 3.393        | 2.835        | 4.344        |
| U-load  | -0.231       | 4.143        | -0.159       | 4.367        |

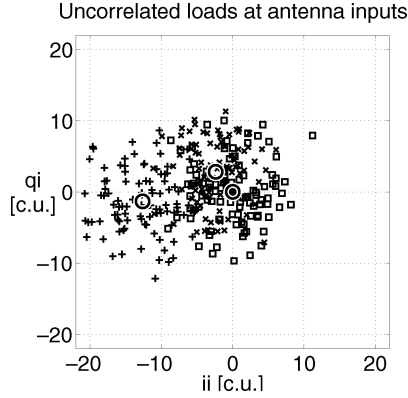


Fig. 9. Result from measurement of uncorrelated loads at antenna inputs. NIR-A mode results are marked with + signs, NIR-TP results with crosses, and U-load results with squares. The circles represent the averages of each measurement. Residual correction has been applied to the results.

### C. Overall Self-Interference

1) *Measurement Setup*: The overall self-interference was measured using an uncorrelated target of an absorber cooled down with liquid nitrogen (LN2). The pyramids of the absorber were about 20 cm long, i.e., close to the wavelength, and NIR was calibrated when the pyramids were nearly under the surface of the LN2. It is acknowledged that this kind of load has its disadvantages since the high level of LN2 reduces the effect of the pyramids. However, the method was considered to be accurate enough to produce an estimate for the magnitude of self-interference. The different levels of brightness temperature were achieved by letting the load to warm up and measuring the load simultaneously using the calibration performed at the beginning.

2) *Results*: Fig. 10 shows the magnitude of the overall self-interference as a function of input noise temperature. Internal and external self-interferences seem to be on the same order of magnitude. The RMS deviation of the measurements from the modeled line is 0.57 c.u. equalling about 0.1 K in Stokes parameters, which is considered quite good.

## VIII. CONCLUSION

The operation principle of the MIRAS reference radiometer, implemented as fully polarimetric noise injection radiometer, was presented. One of the central ideas of the NIR is the so-called blind correlation method, which was demonstrated with measurements. The measurement technique makes the Stokes parameters highly sensitive to the modulus terms, in-

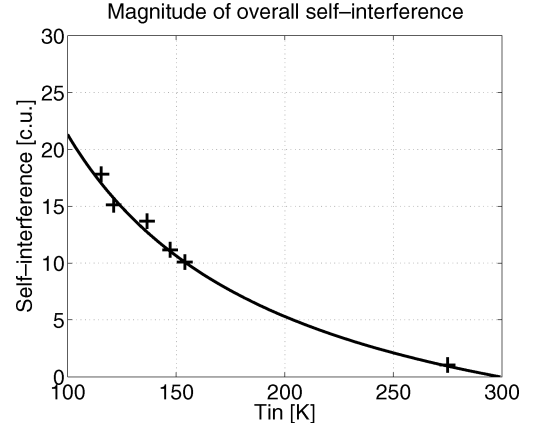


Fig. 10. Magnitude of the overall self-interference determined using absorber load in liquid nitrogen. The crosses are actual measurement results to which the line is fitted.

cluding the amplitude of the noise injection, which have to be measured very accurately.

The calibration procedure of the MDPP-2 noise injection radiometer was also presented. The procedure involves the calibration of the digital correlator, solving of the fringe-washing factor, determination of the offsets created by the receivers and the noise injection operation, and calibration of brightness temperature measurement using the one-point calibration.

Finally measurement results demonstrating the offsets and internal and overall self-interferences were presented. The conclusion is that the self-interference is a significant factor in the measurements, but can be compensated for when using the proper measurements.

## APPENDIX

### A. Equations for Antenna Temperature Measurement and Calibration

The equation for antenna temperature (5) is retrieved starting from the balancing equation of the NIR-A mode as follows: the balancing equation can be written as

$$T_U = \tau T''_{A|ON} + (1 - \tau) T''_{A|OFF} \quad (39)$$

where  $T_U$  is the noise temperature of the internal load,  $T''_{A|ON}$  is the antenna temperature at the receiver input when the noise injection is on, and  $T''_{A|OFF}$  is the antenna temperature at the input of the receiver when the noise injection is off. The antenna temperature at the input of the receiver can be written as

$$T''_A = \frac{T'_A + T'_{N2}}{L_{NC}} + \left(1 - \frac{1}{L_{NC}}\right) T_{p5} \quad (40)$$

where  $T'_A$  is the antenna temperature at the input of the directional coupler,  $T'_{N2}$  is the injection noise in the antenna branch,  $L_{NC}$  is the loss of the directional coupler, and  $T_{p5}$  is the physical temperature of the directional coupler. The antenna temperature at the input of the directional coupler can be written as

$$T'_A = \frac{T_A}{L_A} + \left(1 - \frac{1}{L_A}\right) T_{p5} \quad (41)$$

where  $T_A$  is the antenna temperature and  $L_A$  is the loss of the connection from the antenna to the coupler. The injection noise in the antenna branch is calculated as

$$T'_{N2} = \frac{T_{N2} - T'_A}{F_{NC}} \quad (42)$$

where  $T_{N2}$  is the injection noise at the injection input of the directional coupler and  $F_{NC}$  is the coupling factor of the directional coupler. When the noise injection is on,  $T_{N2}$  can be written as

$$T_{N2|ON} = \frac{T_N}{L_{NA}L_{ON}} + \left(1 - \frac{1}{L_{NA}L_{ON}}\right) T_{p3} \quad (43)$$

where  $T_N$  is the output of the noise source,  $L_{NA}$  is the attenuation of the attenuator in the injection channel, and  $T_{p3}$  is its physical temperature and  $L_{ON}$  is the insertion loss of the switch controlling the noise injection. When the noise injection is off,  $T_{N2}$  can be written as

$$T_{N2|OFF} \approx T_{p3} \quad (44)$$

since the effect of the noise leaking through the switch ( $L_{OFF}$ ) and the directional coupler can be considered negligible.

Now using the balancing equation and the results above, (5) can be retrieved. Also, (36) can be derived using the expressions above.

### B. Equations for NDN Temperature Measurement and Calibration

The equation for NDN noise temperature measurement (26) is retrieved starting from the balancing equation of the NIR-R mode as follows: the balancing equation can be written as

$$T_{NDN} = \tau T''_{ref|ON} + (1 - \tau) T''_{ref|OFF} \quad (45)$$

where the noise temperature of the reference branch when the noise injection is on is defined as

$$T''_{ref|ON} = \frac{T_N}{L_{ON}L_{ref}} + \left(1 - \frac{1}{L_{ON}L_{ref}}\right) T_{p3} \quad (46)$$

and the noise temperature of the reference branch when the noise injection is off is defined as

$$T''_{ref|OFF} = \frac{T_N}{L_{OFF}L_{ref}} + \left(1 - \frac{1}{L_{OFF}L_{ref}}\right) T_{p3} \quad (47)$$

in which  $T_N$  is the output of the noise source,  $L_{OFF}$  is the isolation of the noise injection switch, and  $L_{ref}$  is the attenuation of the attenuator in the reference branch.

Now using the balancing equation and the expressions above, (26) can be retrieved.

For the calibration of the NIR-R mode, first the noise level in the antenna branch during the noise injection is solved using the NIR-A mode. The balancing equation of the NIR-A mode can be written as

$$T_U = \tau T_{Aref} + (1 - \tau) T''_{A|OFF} \quad (48)$$

where  $T_{Aref}$  is the noise level in the antenna branch when the noise injection is on and  $T''_{A|OFF}$  is the same as in (39). From this it yields

$$T_{Aref} = \frac{T_U}{\tau} + \left(1 - \frac{1}{\tau}\right) T''_{A|OFF} \quad (49)$$

from which (37) follows.

Now the noise source output can be determined using REF-CAL mode, the balancing equation of which can be written as

$$T_{Aref} = \tau T''_{ref|ON} + (1 - \tau) T''_{ref|OFF} \quad (50)$$

which yields

$$T_{Aref} = \tau \left( \frac{T_N - T_{p3}}{L_{ON}L_{ref}} + T_{p3} \right) + (1 - \tau) \left( T_{p3} + \frac{T_N - T_{p3}}{L_{OFF}L_{ref}} \right) \quad (51)$$

from which  $T_N$  can be solved yielding (38).

Note that the same noise source output  $T_N$  is solved in two ways for both NIR-A and NIR-R modes separately. This is due to the fact that the accuracy in which the attenuations  $L_{NA}$  and  $L_{ref}$  are known is limited. However, using noise source output for retrieving the antenna and NDN noise temperatures yields the best results despite the inaccuracy of the attenuations. This has been shown by both simulations and experiments.

### ACKNOWLEDGMENT

The authors would like to thank M. Martín-Neira (European Space Agency) and J. Capdevila (European Aeronautic Defence and Space Company-CASA) for valuable comments during the MDPP-2 project.

### REFERENCES

- [1] P. Silvestrin, M. Berger, Y. Kerr, and J. Font, "ESA's second earth explorer opportunity mission: The Soil Moisture and Ocean Salinity mission - SMOS," *IEEE Geosci. Remote Sens. Newslett.*, no. 118, pp. 11-14, Mar. 2001.
- [2] M. Martín-Neira and J. M. Goutoule, "A two-dimensional aperture-synthesis radiometer for soil moisture and ocean salinity observations," *ESA Bull.*, no. 92, pp. 95-104, Nov. 1997.
- [3] F. Ulaby, R. Moore, and A. Fung, *Microwave Remote Sensing, Active and Passive*. Reading, MA: Addison-Wesley, 1981, vol. 1, Fundamentals and Radiometry.
- [4] L. Tsang, J. A. Kong, and R. T. Shin, *Theory of Microwave Remote Sensing*. New York: Wiley, 1999.
- [5] J. B. Hagen and D. T. Farley, "Digital-correlation techniques in radio science," *Radio Sci.*, vol. 8, no. 8-9, pp. 775-784, 1973.
- [6] J. H. Van Vleck and D. Middleton, "The spectrum of clipped noise," *Proc. IEEE*, vol. 54, no. 1, pp. 2-19, Jan. 1966.
- [7] A. Camps, F. Torres, I. Corbella, J. Bara, and J. A. Lluch, "Threshold and timing errors of 1 bit/2 level digital correlators in earth observation synthetic aperture radiometry," *Electron. Lett.*, vol. 33, no. 9, Apr. 1997.
- [8] F. Torres, A. Camps, J. Bara, I. Corbella, and R. Ferrero, "On-board phase and modulus calibration of large aperture synthesis radiometers: Study applied to MIRAS," *IEEE Trans. Geosci. Remote Sens.*, vol. 34, no. 4, pp. 1000-1009, Jul. 1996.
- [9] A. Camps, F. Torres, J. Bara, I. Corbella, and F. Monzon, "Automatic calibration of channels frequency response in interferometric radiometers," *Electron. Lett.*, vol. 35, no. 2, pp. 115-116, Jan. 1999.
- [10] I. Corbella, A. Camps, F. Torres, and J. Bara, "Analysis of noise-injection networks for interferometric radiometer calibration," *IEEE Trans. Microw. Theory Tech.*, vol. 48, no. 4, pp. 545-552, Apr. 2000.



**Andreas Colliander** was born in 1976 in Imatra, Finland. He received the M.Sc. degree from the Helsinki University of Technology (TKK), Espoo, Finland, in 2002.

He is currently a Research Scientist and Project Manager in the Laboratory of Space Technology of TKK, and pursuing his studies toward the D.Sc. degree. He has a research student position in the national Graduate School for Remote Sensing, which is supported by Finnish Ministry of Education and Academy of Finland. His research is focused on microwave radiometer systems, with emphasis on polarimetric and interferometric radiometers, and on theoretical simulation of rough surface backscattering. He has authored and coauthored 11 scientific publications on microwave remote sensing.

Mr. Colliander received the 2002 TKK Master's Thesis Award, an annual award for top five Master's thesis of TKK.

**Simo Tauriainen**, photograph and biography not available at the time of publication.



**Tuomo I. Auer** was born in Pori, Finland, on January 21, 1962. Currently he is writing his masters thesis at the Helsinki University of Technology (HUT), Laboratory of Space Technology, Helsinki, Finland, dealing with digital correlator design and data acquisition of HUT2-D aperture synthesis radiometer.

While studying, he was with Lemminkäinen Ltd. as a Programmer and as an Electronic Designer with Meltron Ltd. (presently MTG-Meltron Ltd.) designing lightning control devices. He has also worked freelance with various electronic projects. Since

1995, he has been with the HUT Laboratory of Space Technology, working on radiometer systems projects (93-GHz imaging radiometer, ESA-MIRAS pilot projects, HUT-2D aperture synthesis radiometer). His current interests include FPGA designs and embedded microcomputer systems.



**Juha Kainulainen** was born in Lappajärvi, Finland, in 1979. He received the M.Sc. degree in technology from the Helsinki University of Technology (HUT), Helsinki, Finland, in 2004.

Since 2001, he has been involved in development and testing of calibration and image reconstruction algorithms used in synthetic aperture radiometers. Currently, he is a Trainee in the Directorate of Earth Observation Programmes at the European Space Agency.

**Josu Uusitalo**, photograph and biography not available at the time of publication.



**Martti Toikka** was born in Rymättylä, Finland, in 1952. He received the M.Sc. degree in electrical engineering from the Helsinki University of Technology (HUT), Helsinki, Finland, in 1979, and the Lic.Tech. degree in 1989.

Since his graduation, he has been working at the HUT Radio Laboratory and after 1986 in the new Laboratory of Space Technology. Since 1995, he has been working as Managing director of Toikka Engineering Ltd. Established in 1986, it is a family-owned RF- and microwave-consulting company, designing

and manufacturing instruments for remote sensing.

His research interests include dielectric properties of materials, microwave radiometer and radar systems, and remote sensing of snow and ice.



**Martti T. Hallikainen** (M'83-SM'85-F'93) received the M.S. degree in engineering and the Dir. Tech. degree from the Faculty of Electrical Engineering, Helsinki University of Technology (HUT), Espoo, Finland, in 1971 and 1980, respectively.

Since 1987, he has been a Professor of Space Technology at HUT, where his research interests include remote sensing and satellite technology. In 1988, he established the HUT Laboratory of Space Technology and serves as its Director. He was a Visiting Scientist from 1993 to 1994 at the European

Union's Joint Research Centre, Institute for Remote Sensing Applications, Ispra, Italy. He was a Postdoctoral Fellow at the Remote Sensing Laboratory, University of Kansas, Lawrence, from 1981 to 1983, and was awarded an ASLA Fulbright Scholarship for graduate studies at the University of Texas, Austin, in 1974-1975. He is an author/coauthor of over 500 scientific publications.

Dr. Hallikainen served as President of IEEE Geoscience and Remote Sensing Society (IEEE GRSS) in 1996 and 1997, and as Vice President in 1994 and 1995. Since 1988, he has been a member of the IEEE GRSS Administrative Committee, and from 1999 to 2001, he served as the IEEE GRSS Nominations Committee Chair and since 2002, as the Fellow Search Committee Chair. He was the General Chairman of the IGARSS'91 Symposium and Guest Editor of the Special IGARSS'91 Issue of the IEEE TRANSACTIONS ON GEOSCIENCE AND REMOTE SENSING (TGARS). Since 1992, he has been an Associate Editor of TGARS. He was a member of the IEEE Periodicals Committee in 1997 and Corresponding member of the IEEE New Technology Directions Committee from 1992 to 1995. He was Secretary General of the European Association of Remote Sensing Laboratories (EARSeL) from 1989 to 1993 and Chairman of the Organizing Committee for the EARSeL 1989 General Assembly and Symposium. He has been a member of the EARSeL Council since 1985, and he was a member of the Editorial Board of the EARSeL Advances in Remote Sensing from 1992 to 1993. He has been a member of the European Space Agency's (ESA) Earth Science Advisory Committee since 1998 and a member of the ESA SMOS Scientific Advisory Group since 2000. He was a national delegate to the ESA Earth Observation Scientific and Technical Advisory Group (EOSTAG) from 1988 to 1994, and he has served in the same capacity on the ESA Earth Observation Data Operations Scientific and Technical Advisory Group (DOSTAG) since 1995. He was Thematic Coordinator of the ESA EMAC-95 airborne campaign for Snow and Ice activities. He was a member of the ESA Multi-frequency Imaging Microwave Radiometer (MIMR) Expert Group from 1988 to 1994 and was a member of the ESA MIMR Scientific Advisory Group from 1994 to 1996. Since 1992, he has been a member of both the Advisory Committee for the European Microwave Signature Laboratory of the European Union's Joint Research Centre and the National Liaison of the International Space University. He is currently serving as Chair of Commission F International Union of Radio Science (URSI) from 2002 to 2005 and has served as its Vice Chair from 1999 to 2002. He was a member of the URSI Long Range Planning Committee from 1996 to 1999, a member of the URSI Committee on Geosphere and Biosphere Program from 1989 to 1999, and a URSI representative to SCOR from 1999 to 2002. He has been a national official member of URSI Commission F (Wave Propagation and Remote Sensing) since 1988. He was Secretary of the Organizing Committee for the URSI Nordic Antenna Symposium in 1976, and he served as Secretary of the Finnish National Committee of URSI from 1975 to 1989. He was Vice Chair of the URSI Finnish National Committee from 1990 to 1996, and he has served as its Chair since 1997. He is Vice Chair of the Finnish National Committee of COSPAR since 2000. He is the recipient of three IEEE GRSS Awards: 1999 Distinguished Achievement Award, IGARSS'96 Interactive Paper Award, and 1994 Outstanding Service Award. He is the winner of the Microwave Prize for the best paper in the 1992 European Microwave Conference, and he received the HUT Foundation Award for excellence in research in 1990. He and his research team received the 1989 National Research Project of the Year Award from *Tekniikka & Talous (Technology & Management Magazine)*. He received the 1984 Editorial Board Prize of Sähkö—Electricity in Finland.